Published in final edited form as:
Neuropathol Appl Neurobiol. 2010 October ; 36(6): 462–477. doi:10.1111/j.1365-2990.2010.01103.x.

Tyrosine phosphorylation of tau accompanies disease progression in transgenic mouse models of tauopathy

Kiran Bhaskar[1,*], **G. Aaron Hobbs**[1,+], **Shu-Hui Yen**[2], and **Gloria Lee**[1]

[1]Department of Internal Medicine, University of Iowa Carver College of Medicine, Iowa City, IA 52242

[2]Department of Neuroscience, Mayo Clinic Jacksonville, Jacksonville, FL 32224, USA

Abstract

Aim—Tau protein is a prominent component of paired helical filaments in Alzheimer's disease (AD) and other tauopathies. While the abnormal phosphorylation of tau on serine and threonine has been well established in the disease process, its phosphorylation on tyrosine has only recently been described. We previously showed that the Src family non-receptor tyrosine kinases (SFKs) Fyn and Src phosphorylate tau on Tyr18 and that phospho-Tyr18-tau was present in AD brain. In this study, we have investigated the appearance of phospho-Tyr18-tau, activated-SFK, and Proliferating Cell Nuclear Antigen (PCNA) during disease progression in a mouse model of human tauopathy.

Methods—We have used JNPL3, which expresses human tau with P301L mutation, and antibodies specific for phospho-Tyr18-tau (9G3), ser/thr phosphorylated tau (AT8), activated-SFK, and PCNA. Antibody staining was viewed by either epifluorescence or confocal microscopy.

Results—Phospho-Tyr18-tau appeared concurrently with AT8-reactive tau as early as 4 months in JNPL3. Some 9G3-positive cells also contained activated-SFKs and PCNA. We also investigated the triple transgenic mouse model of AD and found that unlike the JNPL3 model, the appearance of 9G3 reactivity did not coincide with AT8 in the hippocampus, suggesting that the presence of APP/presenilin influences tau phosphorylation. Also, thioflavin-S positive plaques were 9G3 negative, suggesting that phospho-Tyr18 tau is absent from the dystrophic neurites of the mouse triple transgenic brain.

Conclusions—Our results provide evidence for the association of tyrosine-phosphorylated tau with mechanisms of neuropathogenesis and indicate that SFK activation and cell cycle activation are also involved in JNPL3.

Keywords

tyrosine-phosphorylated tau; Src family tyrosine kinases; tauopathy mouse model; AT8; Proliferating Cell Nuclear Antigen; tau hyperphosphorylation

Introduction

The microtubule-associated protein tau is the primary component of the neurofibrillary tangles found in several age related neurodegenerative diseases such as Alzheimer's disease (AD). While the phosphorylation of tau on serine and threonine residues during

Correspondence: Dr. Gloria Lee gloria-lee@uiowa.edu.
[*]Current address: Department of Neurosciences, The Cleveland Clinic Foundation, Cleveland, OH 44195
[+]Current address: Department of Biochemistry and Biophysics, University of North Carolina, Chapel Hill, NC 27599

neuropathogenesis has been well established (reviewed by [1]), the tyrosine phosphorylation of tau in AD has only been recently described [2-4]. Tau is phosphorylated by Fyn, Src and Lck, members of the Src family non-receptor tyrosine kinase family (SFK) [2,4] as well as by Abl and Syk [3,5]. Fyn has been proposed to have a role in disease pathogenesis based on data obtained from AD patient samples [6,7]. In addition, Fyn depletion conferred protection against neurotoxicity induced by Aβ [8] and reduced the synaptotoxicity and neurotoxicity exhibited by a transgenic mouse overexpressing human amyloid precursor protein [9]; Fyn over-expression in the same mouse model potentiated behavioral deficits [9]. These findings have suggested that tyrosine phosphorylation is an important component in the neurodegenerative disease process.

Tau neuropathology is also found in frontotemporal dementia with parkinsonism linked to chromosome 17 (FTDP-17) and several of these diseases are caused by mutations in the tau gene (reviewed by [10]). We have demonstrated that either the tau missense mutations that cause FTDP-17 or disease-related ser-thr phosphorylation increased the interaction of a four-repeat tau isoform with the SH3 domain of Fyn [11]. As this interaction directs the tyrosine phosphorylation of tau on tyrosine 18, it might be expected that tauopathy mutations or disease-related phosphorylation would promote the phosphorylation of four-repeat tau on Tyr18. To investigate this further, we have used the P301L JNPL3 mouse tauopathy model that expresses four-repeat tau with P301L, an FTDP-17 mutation. P301L tau is expressed at levels that approximate endogenous tau levels, thereby doubling total tau levels, and JNPL3 exhibits both abnormally phosphorylated tau and insoluble tau species at 3 months, as detected by biochemical methods [12,13]. Neurofibrillary tangles occur most prominently in the spinal cord and brain stem, spreading to other areas in an age-dependent manner and granular tau immunoreactivity commonly appears in the hippocampus, cortex, and basal ganglia [13]. Besides tau pathology, JNPL3 has marked gliosis, axonal degeneration, neuronal loss, and motor impairment [13]. In previous work, using a probe against phospho-Tyr18 in tau (monoclonal 9G3), we had found tyrosine phosphorylated tau in JNPL3 at 8 months [11], thus confirming the presence of tyrosine phosphorylated tau in a model for age-related neurodegenerative disease. This finding, in turn, raised the question of how the appearance of tyrosine phosphorylated tau would correlate with the progression of tau pathology. Also of interest was the possible activation of Src family tyrosine kinases (SFKs) as we had found that tau can enhance the activation of SFK [14]. Here we describe the temporal and spatial distribution of Tyr18 phosphorylated (9G3 positive) tau in the JNPL3 mouse model [13] and compare it to that of Ser202/Thr205 phosphorylated tau, as detected by AT8, an established marker of tau pathology. We also compare the temporal and spatial distribution of tyrosine phosphorylated tau to that of activated SFK.

Because SFK are oncogenes that can lead to the loss of cell cycle control, we also investigated the appearance of Proliferating Cell Nuclear Antigen (PCNA), a marker for activated cell cycle. Activated cell cycle markers have been described in several neurodegenerative disorders [15,16] and a loss of cell cycle control has been proposed as a mechanism for neuronal death [17,18]. Two tauopathy mouse models have shown expression of cell cycle markers indicative of re-entry into the cell cycle [19,20] and tau-induced neuronal loss has been shown to require genes that promote cell cycle progression [21]. Here we use the JNPL3 mouse to determine if cells containing tyrosine phosphorylated tau, which would be indicative of activated tyrosine phosphorylation, might also have a loss of cell cycle control, as detected by the presence of PCNA.

Studies performed in mouse tauopathy models have reported that the presence of amyloid pathology exacerbates tau pathology [22,23]. Because the Aβ peptide in the amyloid pathology of AD is an extracellular entity that can potentially trigger signaling pathways that could activate tyrosine phosphorylation, we were interested in comparing the tyrosine

phosphorylation of tau in JNPL3 with that in a mouse model which had both Aβ pathology and neurofibrillary tangles. The "triple transgenic" mouse model (3xTg), that also expresses P301L tau as well as mutant human APP and PSEN1 [24], is well suited for this purpose. The 3xTg model develops both amyloid and tau pathologies in an age-related manner where Aβ plaque formation precedes neurofibrillary tangle formation [24]. Moreover, clearance of Aβ with anti-Aβ antibodies significantly reduces tau pathology [25]. To investigate the effect of Aβ pathology on tyrosine phosphorylation of tau, we extended our analysis of tyrosine phosphorylated tau into the 3xTg model. Our results show that the tyrosine phosphorylation of tau in this model differs relative to that found in JNPL3.

Materials and Methods

Immunofluorescence

4-, 6- and 8-month-old heterozygous JNPL3 and 10-, 11- and 12-month old homozygous 3xTg mouse brains (n=3 per age group) were harvested for immunohistochemistry. 5μm thick paraffin sections were incubated with monoclonal antibodies 9G3 (specific for tau phosphorylated at Tyr18), AT8 (specific for tau phosphorylated at Ser202/Thr205 (1:200; Pierce, Rockford, IL)), or disease-related conformation specific antibodies TG3 or Alz50 (1:10; gift of P. Davies). In JNPL3 mice, activated SFK was detected by an antibody against phosphorylated Src tyrosine 416 (mouse monoclonal clone 9A6; Upstate, Billerica, MA). A very low basal level of activated-SFK immunoreactivity was observed throughout the brain sections at all JNPL3 age groups examined. Cells were considered "positive" for activated SFK when the intensity was significantly higher than the basal level. Cells in early G1/S phase of the cell cycle were detected using anti-PCNA antibody (Abcam, Cambridge, MA). For sequential immunofluorescence labeling of mouse brain sections, phosphorylation of Tyr18 was detected using biotinylated 9G3 [4] and streptavidin-Alexa488 (Molecular Probes, Carlsbad, CA) following AT8, TG3, Alz50, anti-PCNA or anti-activated SFK detection with rhodamine conjugated donkey anti-mouse secondary antibody (Jackson Immunochemicals, West Grove, PA). For Thioflavin S and 9G3 sequential labeling in 3xTg mouse, Thioflavin S (Sigma, St. Louis, MO) staining was performed by rehydrating the brain sections and staining in 1% Thioflavin S for 5 min, followed by staining with 9G3 and Alexa546-anti-mouse secondary antibody. For Aβ and 9G3 double labeling, the sections were sequentially labeled with anti-Aβ antibody 6E10 (Covance, Princeton, NJ) followed by biotinylated-9G3. Since 6E10 also recognizes full-length APP, we used 6E10 at 1:1000 dilution, as reported by Oddo et al. [24], to optimize the signal to noise ratio for the detection of intracellular Aβ and to minimize the basal level of staining contributed by full length APP. DAPI or Hoechst was used to stain nuclei. Background controls using no primary or no secondary, as well as unstained sections, revealed no signficiant background staining or autofluorescence. Immunostained sections were observed by epifluorescence (Nikon E800) or confocal microscopy (BioRad 1024).

For quantitation, fifteen sections per mouse were evaluated. The sections were taken at different coronal planes covering areas of the brain stem, lateral hippocampus, anterior commissure and olfactory bulb (Fig. S1); sections were otherwise randomly chosen. For counting, areas were sampled from the brain stem, hippocampus, subcortical structures (at the levels of anterior commissure/basal ganglia and diencephalon), and entorhinal/piriform cortices. These areas were chosen because pre-tangle forms of tau immunoreactivity occurred widely in these areas, randomly distributed [11]. For counting, each section was first divided into rectangular fields using an eye-piece reticule, then each field was examined for cells positive for phospho-Tyr18 tau alone or for both phospho-Tyr18 tau and other antigens described. In parallel, the number of cells per field was counted using Hoechst staining; this count would include both neuronal and non-neuronal cells. From the brain stem, approximately 16+1 fields (containing 4550+227 cells) per section were examined.

From the subcortical structure, 70±4 fields (containing 1440±72 cells) per section were examined. From the hippocampus, 42±3 fields (containing 2638±131 cells) per section were examined. From the entorhinal/piriform cortex, 26+2 fields (containing 1040±52 cells) per section were examined. The total number of positive cells was averaged per age group and the percentage of positive cells was calculated as follows: 1) for 9G3 and AT8 single labeling – total number of cells as labeled by Hoechst were counted per brain region per age group and was assigned 100%. 2) For 9G3+Active-Src double labeling – sum of cells positive for 9G3 only, 9G3+Active Src, and Active Src only per brain region per age group was assigned 100%. 3) For PCNA and 9G3 double labeling – sum of cells positive for 9G3 only, 9G3+PCNA, and PCNA only per brain region at 8-months was assigned 100%. Statistical analysis was performed using unpaired *t*-test or one-way ANOVA and correlation analysis was performed using InStat® software. Because we have used a nonstereological method to quantify the number of immunoreactive cells, it is important to point out that based on the Hoechst staining used to determine the total number of cells present, the number of immunoreactive cells quantified was three to five percent of the total Hoechst positive cells scored. Therefore, immunoreactive cells were distinctly identifiable and well separated from their closest neighboring positive cells, minimizing the possibility of counting immunoreactive cells twice. Furthermore, the data has been presented either as a percentage of the total number of cells present, as detected by Hoechst staining (Fig. 1b, 1c, 1d), or as a percentage of the total number of immunoreactive cells, when more than one epitope was being assessed (Fig. 4m, Table 1). Therefore, as stained cells were normalized relative to other stained cells, differences in cell density between different anatomical areas were factored out. At the same time, it should be noted that such an approach does not quantitate the amount of antibody reactivity per area or volume of brain tissue and would not be suitable if one were interested in the absolute amount of antigen present, as staining intensity and cell sizes were not quantitated. Nevertheless, this method of quantification has been used in other studies to quantify pyknotic or eosinophilic dying neurons, Flouro-Jade positive neurons, TUNEL positive cells and sensory neurons [26,27].

Immunoelectron microscopy

Ultrathin sections of spinal cords from 15-month-old JNPL3 transgenic mouse were processed for post-embedding immunoelectron microscopy to detect phospho-Tyr18 tau using 9G3. Goat anti-mouse secondary antibody conjugated to 10nm gold particles (Aurion, Wageningen, The Netherlands) was used for detection. The grids were counterstained with uranyl acetate (saturated solution in 70% ethanol; pH 4.2) for 90 min and lead citrate (0.2% pH 12.0) for 5 min and observed in Joel TEM (JEM-1230).

Results

Expression of phospho-Tyr18 tau increases with age in JNPL3 transgenic mouse brain

The temporal expression of phospho-Tyr18 tau in different brain regions of the JNPL3 mouse brain was determined using immunofluorescence labeling with 9G3, a probe specific for phospho-Tyr18 tau [4]. While our earlier results in JNPL3 had demonstrated the presence of phospho-Tyr18 tau at 8 months by immunofluorescence staining [11], at 3 months tyrosine-phosphorylated tau was absent as detected by immunoprecipitation methods [28]. Therefore, we tested for the appearance of 9G3 positive cells at 4 months, and found positive cells in layer II and III of the entorhinal cortex, displaying diffuse cytoplasmic staining in the cell body (Fig. 1). At this time, 9G3 positive cells were also found in the brain stem and sub-cortical structures, but at lower numbers. Between 4 and 8 months, the density of 9G3 positive cells increased in the entorhinal cortex (Fig. 1a insets). At 8 months, 9G3 positive cells appeared in the deeper layers of entorhinal cortex while the number of positive cells increased in the hippocampus, brain stem, and subcortical structures. We did

not detect any 9G3 positive cell clusters within the subcortical structures or the brain stem; cells positive for phospho-Tyr18 were randomly distributed across a wider area within each structure. However, we noted that the CA1 neurons of the hippocampus and the subiculum, as well as pyramidal neurons in the entorhinal cortex, were positive for phospho-Tyr18 tau. The identity of cells as neurons was based on their size and shape. In contrast, phospho-Tyr18 tau was completely absent in 8-month-old non-transgenic brain sections (Fig. 1a, Non-Tg).

Next we quantified the percent of 9G3 immunoreactive cells in the entorhinal cortex, brain stem, hippocampus and subcortical structures in 4-, 6- and 8-month-old JNPL3 mouse brain. Fields with immunoreactive cells were sampled to obtain counts of cells stained with 9G3 and counts of cell nuclei stained with Hoechst, which would yield total cell number. At 4 months, the percent of 9G3-positive cells ranged from <0.01% (hippocampus) to 0.5% (entorhinal cortex) and increased at 6 and 8 months (Fig. 1b). Among the four regions examined, the entorhinal cortex initially displayed the highest percent of 9G3-positive cells. However, at 6 and 8 months, while the number of positive cells in the entorhinal cortex increased, the differences were not statistically significant. In contrast, at these time points the increases in 9G3 immunoreactive cells in the hippocampus and subcortical structures were statistically significant (Fig. 1b). At 8 months, the number of cells with phospho-Tyr18 tau was highest in entorhinal cortex and subcortical structures, with the latter showing a significantly higher number of 9G3 positive cells as compared to hippocampus and the brain stem (Fig. 1b).

Appearance of phospho-Tyr18 tau correlates with the appearance of phospho-Ser202/Thr205 in JNPL3 mice

Phospho-Ser202/Thr205 tau, as detected by the antibody AT8, labels granular cytoplasmic, prefibrillar material in Alzheimer's disease [29] and appears in several P301L transgenic mouse models, including JNPL3 [13,30,31]. To determine if the appearance of phospho-Tyr18 tau temporally correlated with the appearance of phospho-Ser202/Thr205 positive tau, we quantified the number of cells positive for AT8, using the same protocol as applied previously for 9G3, examining four regions of the JNPL3 mouse brain at 4, 6, and 8 months of age. When data for 9G3 and AT8 were plotted together, their temporal and spatial expression patterns were similar (Fig. 1c). This was confirmed by performing Spearman rank correlation and linear regression analysis for the two data sets. We found that the increase in the percentage of 9G3-positive cells was significantly correlated with the increase in the percentage of AT8-positive cells in the different brain regions of the three age groups studied (Fig. 1d; Spearman Rank, $r^2=0.84$, n=12; $p<0.0001$). These results suggested that in the P301L mouse brain, phosphorylation of tau on Tyr18 is spatially and temporally regulated in a manner that is similar to that regulating Ser202/Thr205 phosphorylation.

Previously, we had reported that 9G3 and AT8 double-labeled neurons in the entorhinal cortex of 8-month old JNPL3 mouse brain [11]. To determine if co-localization of these two phosphorylated tau forms extended to other brain regions as well as to earlier stages of the disease, we performed double-label immunofluorescence with 9G3 and AT8 on 4, 6, and 8 month old JNPL3 mouse brain sections. Cells positive for both AT8 and phospho-Tyr18 tau were present in the entorhinal cortex of all samples (Fig. 2a). Double-labeled cells were also seen in hippocampus, subcortical structures and brain stem of 8-month old JNPL3 mouse brain (not shown). Singly labeled cells, showing only AT8 or 9G3 labeling, were absent. On a subcellular level, AT8 and 9G3 showed an identical labeling pattern. In addition, we observed that 9G3-positive cells in the entorhinal cortex were also positive for TG3, a conformation-specific antibody recognizing phospho-Thr231 (data not shown), and Alz50, a disease-related conformation specific antibody. We noted that although Alz50 and 9G3

appeared in the same cell, their subcellular distribution appeared different. By using confocal microscopy to examine z-series of double stained cells, we found that the Alz50 and 9G3 reactivities peaked at different parts of the cell and that Alz50 was cytosolic while 9G3 appeared closer to the plasma membrane (Fig. 2a, bottom row).

As an additional demonstration that phospho-Tyr18 tau occurred as an integral part of the neuropathology of the JNPL3 mouse, we examined mature neurofibrillary tangles at the ultrastructural level. Both 15-20 nm straight filaments and filamentous aggregates with a herringbone pattern have been previously observed in the spinal cord of the JNPL3 model using electron microscopy [32]. By probing ultrathin sections from the same sample with 9G3 and immunogold, we found that both filament types were labeled by 9G3 (Fig. 2b), indicating that tau filaments were tyrosine phosphorylated.

Expression of phospho-Tyr18 tau differs from that of AT8-reactive tau in the 3xTg transgenic mouse model of AD

The 3xTg mouse model demonstrates amyloid plaques, in addition to neurofibrillary tangles. In the 3xTg mouse model, we first observed AT8-reactive tau at 10 months, localizing in the fimbria (Fig. 3a) and subicular regions, corpus callosum, and the entorhinal cortex (not shown). At 12 months, AT8-reactive tau was also observed in subiculum (Fig. 3b) and subcortical structures (not shown). In contrast, we first observed 9G3-reactive tau at 12 months, localizing in the CA1 region of the hippocampus (Fig. 3c) and entorhinal cortex (not shown). While AT8 positive cells were not necessarily 9G3 positive, all 9G3 positive CA1 pyramidal cells were also labeled by AT8 (Fig. 3d). Overall, in 12-month-old 3xTg mice, the incidence of 9G3 positive cells, as well as AT8 positive cells, was far below that of the 8-month-old JNPL3 mice.

To determine whether phospho-Tyr18 tau localizes to cells rich in soluble and intracellular Aß and/or to extracellular aggregated Aß, we performed double labeling with 9G3 and either anti-Aβ antibody (6E10) or Thioflavin S in 12 month old 3xTg mouse brain sections. While 6E10 basal staining contributed by full length APP was present, no elevation in 6E10 staining was detected in CA1 hippocampal cells that were immunoreactive for 9G3 (Fig. 3e), suggesting the absence of intracellular Aß. At the same time, Thioflavin S positive dense-core plaques were negative for 9G3 (Fig. 3f). These results suggest that phospho-Tyr18 tau does not co-localize with the Thioflavin S positive Aß plaque or with soluble intracellular Aß in the 12 month old 3xTg mice.

Phospho-Tyr18 tau partially co-localizes with activated Src family kinases (SFK) in JNPL3 mice

We had previously demonstrated that Src family tyrosine kinases (SFKs) phosphorylate tau at Tyr18 [4] and tau, in turn, could potentiate Fyn and Src activation [14]. To investigate the relationship between the appearance of phospho-Tyr18 tau and SFK activation in JNPL3, we performed double-labeling with 9G3 and an antibody specific for the activated form of SFKs (anti-phospho-Tyr416). Three different sets of labeled cell populations were observed in the brain stem of 8-month old JNPL3 mouse. The first set of cells, found in the lateral vestibular nucleus, was positive for activated SFK but negative for phospho-Tyr18 tau (Fig. 4a-c). The second set, found posterior to the vestibular nucleus, was positive for phospho-Tyr18 tau but negative for activated SFK (Fig. 4d-f). The third set was positive for both probes. At 8-months, we also observed the same three sets of cells in the subcortical structures of JNPL3. However, in the hippocampus and entorhinal cortex, only the third set of cells was found, where the cells were positive for both activated-SFK and phospho-Tyr18 tau. Within this set, the cells exhibited two patterns of subcellular localization, one where phospho-Tyr18 tau did not co-localize with activated SFK (Fig. 4g-i) and one where the two species co-

localized (Fig. 4j-l). It is of note that the activated-SFK signal was stronger in cells of the third set relative to those in the first set, suggesting a correlation between the presence of tau and increased activated SFK.

Next we determined the number of cells in each of the above three sets (cells positive for phospho-Tyr18 tau, activated-SFK, or for both) in brain stem, subcortical structures, hippocampus and entorhinal cortex at 4-, 6- and 8-month old JNPL3 brain samples. We assigned 100% to the sum of all positive cells and determined the percent of cells in each of the three groups for each sample. Of the four areas analyzed, the entorhinal cortex, at 4 months, showed the earliest appearance of cells containing activated-SFK; these cells also contained phospho-Tyr18 tau. At this time, these double-labeled cells (Fig. 4m, right panel, red circle) made up roughly half of the cells that contained phospho-tyr-18 tau in the entorhinal cortex. Double-labeled cells were found in the entorhinal cortex at 6 months as well and at 8 months, all 9G3-reactive cells contained activated-SFK, as mentioned above. Following the entorhinal cortex, the subcortical structures were next to show presence of activated-SFK immunoreactive cells at 6 months. Again, these cells were also positive for phospho-Tyr18 tau (Fig. 4m, middle panel, red circle). At this time, the brainstem showed a low percentage of cells containing activated-SFK, with more than half lacking 9G3-reactivity (Fig. 4m, left panel, light blue square). Cells with only activated-SFK did not appear in subcortical structures until 8 months. In contrast, cells with only activated-SFK were absent from entorhinal cortex and hippocampus at all ages examined. As shown above, 9G3-reactive cells first appeared in the hippocampus at 8 months and we found that these cells all contained activated SFK, similar to the entorhinal cortex at 8 months (data not shown). Overall, the number of cells positive for activated-SFK increased with age in all regions.

Phospho-Tyr18 tau partially co-localizes with PCNA in different brain regions of JNPL3 mice

Several neurodegenerative diseases characterized by the presence of filamentous tau inclusions express PCNA, a marker of the S-phase of the cell cycle [16] and PCNA has also been described in a mouse model of tauopathy [19]. As the appearance of cell cycle markers has not been described in JNPL3, we first examined PCNA expression in JNPL3 and non-transgenic mouse brain. At 2, 4, and 6 months, no differences between the numbers of PCNA positive cells in the transgenic versus non-transgenic brains were observed (data not shown). However, at 8 months we observed a noticeable increase in the number of PCNA positive cells in the brain stem, entorhinal cortex and hippocampus of the JNPL3 brain relative to the age-matched non-transgenic control brains. Quantitation of PCNA containing cells indicated that the JNPL3 brainstem contained 8-fold more PCNA positive cells than the non-transgenic brainstem. When we performed double-labeling to quantify phospho-Tyr18 tau and PCNA positive cells in different brain regions, we observed three sets of immunoreactive cells, simlar to those we had previously discerned in our activated-SFK analysis. Cells positive for only phospho-Tyr18 tau (Fig. 5 a, c; green), cells positive for only PCNA (Fig. 5 b,c; red), and cells positive for both (Fig. 5d) were found. However, unlike our previous results with phospho-Tyr18 tau and activated-SFK, cells containing both PCNA and phospho-Tyr18 tau immunoreactivity never exceeded a quarter of the total set of positive cells in any of the brain regions studied (column C, Table 1). The highest fraction of doubly positive cells was found in the brain stem where just more than half of 9G3 positive cells were also positive for PCNA (column D, Table 1). In addition, in the 8 month old hippocampus and entorhinal cortex, where all phospho-Tyr18-tau cells were also positive for activated-SFK, less than a quarter of 9G3 positive cells were positive for PCNA (column D, Table 1).

Discussion

In the JNPL3 mouse model, tyrosine phosphorylated tau appeared at four months and its subsequent pattern of expression was indistinguishable from that of Ser202/Thr205 phosphorylated tau, as detected by AT8. This finding is consistent with our previous data showing that the phosphorylation of 0N4R tau at the AT8 site did not negatively affect its association with Fyn or Src SH3 domain ([11] and unpublished data). However, in the four brain areas sampled in the 8 month old JNPL3, only 1-4% of the cells contained 9G3 staining, suggesting that a very low percentage of total tau is phosphorylated on Tyr18. This may account for the failure of our earlier study to detect phospho-Tyr18 tau in soluble or sarkosyl insoluble fractions from JNPL3 brain [28]. Nevertheless, epifluorescence, confocal, and immunoelectron microscopy data showed that phospho-Tyr18 was presesnt in this model.

We also noted that at the intracellular level, 9G3 immunoreactivity differed spatially from Alz50, suggesting that Tyr18 phosphorylation and the conformational change that generates the Alz50 epitope in tau [33,34], are mutually exclusive. The Alz50 epitope is created by both the extreme amino terminus of tau and a part of its microtubule binding domain and phosphorylation at Tyr18 may prevent the formation of the epitope. Alternatively, the interaction forming the Alz50 epitope may prevent phosphorylation of Tyr18 or promote dephosphorylation of Tyr18. The non-overlapping spatial localizations of the two species suggest that each tau isoform may be engaged in different interactions within the neuron at this time (8 months). This idea is supported by our previous finding that phospho-Tyr18 tau was differentially localized relative to nonphospho-Tyr18 tau in the Alzheimer disease brain [4].

In the 3xTg mouse model, tyrosine phosphorylated tau did not have the same expression pattern as AT8. This could be explained by the fact that the two models use different promoters for expression (prion promoter in JNPL3 and Thy1.2 promoter in 3xTg), which could result in tissue specific differences in tau phosphorylation. However, both promoters are active in the hippocampus, entorhinal cortex, and subcortical structures and therefore, human tau is present in these tissues in both adult mouse models. However, once present, tyrosine phosphorylation coincided with AT8 phosphorylation in the JNPL3 model whereas tyrosine phosphorylation was sometimes absent from cells with AT8 signal in the 3xTg model. We have previously reported the similar absence of tyrosine-phosphorylated tau in the AT8-labeled neuropil threads and dystrophic neurites in the entorhinal cortex of Alzheimer disease brain [4]. In addition, in the hippocampus of JNPL3, tyrosine phosphorylated tau and activated SFK appeared in the same cells whereas in the 3xTg hippocampus, activated SFK did not appear (data not shown). Judging from our data, because the relationship between AT8 and 9G3 reactivity in JNPL3 was altered in 3xTg, the implication is that the presence of APP/PS1 mutants changed the relationship between ser/thr phosphorylation, which determines AT8 reactivity, and tyrosine phosphorylation, which determines 9G3 reactivity. Our findings are also consistent with a role for APP/PS1 in SFK activation because in JNPL3, SFK activation appeared in various locations, as early as 9G3 and AT8, whereas in the 3xTg model, SFK activation was notably absent.

An alternate explanation for our findings might stem from the tau expression level in the 3xTg mouse being lower than that in JNPL3. If true and if SFK activation depended on tau (see below), the net result might be less tyrosine phosphorylated tau and the absence of SFK activation. At the same time, it should be noted that the JNPL3 and 3xTg mice have different genetic backgrounds (C57BL6/DBA/SW for JNPL3 versus C57BL6/129 for 3xTg), which may contribute to temporal and spatial differences in the activated-SFK, phospho-Tyr18 tau, and/or AT8 observed in the present study. Also, it should be pointed out

that the age at which AT8 positive tau first appears in the 3xTg model has not been consistent between laboratories, ranging between 6 and 12 months [35,36]. Because of the variability in staining techniques and possible variability in mouse colonies, comparisons between staining patterns are best performed with data obtained within a single study. Our findings are consistent with a role for APP/PS1 in regulating tau phosphorylation and SFK activation.

In the JNPL3 brain stem and subcortical structures, tyrosine phosphorylated tau appeared in the absence of activated SFK at 4-6 months. Since the 9G3 antibody detects an SFK site on tau (phospho-Tyr18), it is likely that an undetectable increase in the level of activated SFK was sufficient to phosphorylate tau and create 9G3 staining. 9G3 is able to detect phospho-Tyr18-tau with a K_D of 2×10^{-12} M [4] and is therefore a very sensitive reagent. The sensitivity of the activated SFK reagent is unknown. In addition, since SFK is an enzyme, minimal activation may be sufficient to accumulate detectable levels of tyrosine phosphorylated tau. As the number of 9G3 positive cells in the JNPL3 brain stem and subcortical structures increased from 4 to 8 months, the number of cells positive for activated SFK also increased (compare Fig. 1b and 4m). These findings are consistent with both the ability of activated SFK to increase 9G3 reactivity and the ability of tau to increase SFK activation [14].

In the hippocampus and entorhinal cortex of the JNPL3 model, every cell containing activated SFK also contained tyrosine phosphorylated tau whereas this correlation did not exist in the brain stem or subcortical structures. In fact, the brain stem and subcortical structures also contained cells that had only activated SFK without having 9G3-reactive tau. This suggests that the relationship between tau and activated SFK in the hippocampus and entorhinal cortex will be distinct from that in the brain stem and subcortical structures. Such differences are consistent with the selective neuronal vulnerability in human disease. That is, despite the fact that the P301L mutant tau is being expressed in several neuronal cell types, its ability to increase SFK activation, that would, in turn, increase tyrosine phosphorylation of tau, develops in cell-type specific manners. Some cells in the brain stem and subcortical structures, for instance, may have a form of tau that cannot be tyrosine phosphorylated, despite the presence of activated SFK. We have reported that tau phosphorylated at Thr231 does not interact with SFK and is not tyrosine phosphorylated [11,37]. In fact, the presence of phospho-Thr231 has been reported in both JNPL3 and 3xTg models. In JNPL3, phospho-Thr231 was detected in the subcortical brain at 3 months, with the levels decreasing at 6 and 9 months [12]. The decrease coincided with the increases in phospho-Tyr18 tau detected in the subcortical structures at 6 and 8 months (Fig. 1b). In 3xTg, phospho-Thr231 was detected in the hippocampus at 6 months, with increased levels at 9 months, followed by a decrease at 12 months [38]. Interestingly, the decrease corresponded with the time we first detected phospho-Tyr18 in the hippocampus. In addition, the 3xTg entorhinal cortex lacked phospho-Thr231 until 26 months [38], indicating that the appearance of phospho-Tyr18 in entorhinal cortex at 12 months coincided with the absence of phospho-Thr231 in this location. These findings are consistent with the known relationship between phospho-Thr231 and phospho-Tyr18 and provide an example of the different aspects that may influence tyrosine phosphorylation of tau. Different cell types will have differences in signal transduction pathways as well as differences in their responses to the environmental cues encountered by each cell type in its anatomical location.

The presence of activated SFK in the JNPL3 model suggests a role for Fyn or Src in neurodegenerative disease. Evidence for a role for Fyn has already been obtained in the hAPP mouse model of AD [9]. Because constitutively active SFKs are oncogenic and lead to a loss of cell cycle control, we investigated the appearance of PCNA. In the 8 month old JNPL3 entorhinal cortex and hippocampus, we observed that a minority (less than 25%) of

the phospho-Tyr18 tau-containing cells also contained PCNA. However, the number of cells that contained only PCNA exceeded those that had both PCNA and phospho-Tyr18 tau (column B vs. column C, Table 1). These findings suggest that the appearance of PCNA does not require a detectable accumulation of abnormally phosphorylated tau, either AT8 or 9G3 reactive, nor does it require activated SFK, since in the entorhinal cortex and hippocampus at 8 months, activated SFK and 9G3 are in the same cells (Fig. 4m). Nevertheless, since non-transgenic mice did not exhibit PCNA, the presence of tau correlated with the increase in PCNA expression. Our finding is consistent with those reported in a mouse model expressing wild type tau where it was found that although PCNA was detected, it did not co-localize with tau pathology [19]. These findings are also consistent with results obtained in human tauopathies where cell cycle markers such as cyclin B1 occurred in the absence of fibrillar tau [16]. Hoerndli et al. have recently demonstrated that overexpressed human P301L tau altered gene expression in SH-SY5Y cells, up-regulating many proteins, including cell cycle regulators such as PCNA [39]. Based on this study, one would speculate that gene expression in JNPL3 and 3xTg mouse neurons would be altered as well. However, since only some neurons exhibited abnormally phosphorylated tau pathology and/or PCNA, the response of neurons to the presence of tau is clearly diverse in nature.

The presence of ser/thr phosphorylated tau, tyrosine phosphorylated tau, and PCNA in human post-mortem material has been demonstrated. However, the ability to detect activated SFK in human post-mortem brain has not been demonstrated although total Fyn and Src have been examined in human AD cases by Ho et al. [7]. These investigators reported a shift in the subcellular compartmentalization of Fyn during the disease process but did not report changes in Fyn activity due to concerns regarding the accuracy of kinase assays performed on human post-mortem material; activated SFK would be highly susceptible to de-activation by tyrosine protein phosphatases during the post-mortem period. Therefore, despite the limitations in using transgenic mice to model human disease, the mouse models offer the opportunity to probe for labile entities such as activated kinases. Our data supports the hypothesis that the shift in Fyn compartmentalization reported by Ho et al. corresponds to an increase in kinase activation.

In summary, our investigation has shown that tyrosine phosphorylated tau appears similarly with ser/thr phosphorylated tau in the JNPL3 mouse model and that this relationship is altered in the 3xTg mouse model. In addition, activated SFK and PCNA are found in the JNPL3 mouse, consistent with the ability of tau to potentiate SFK activity and to affect the expression of cell cycle related proteins. The appearance of phospho-Tyr18 tau and other disease model attributes for both JNPL3 and 3xTg models are summarized in Fig. 6. In JNPL3, we have observed that phospho-Tyr18 tau positive cells were evident at 4 months in all brain regions studied except the hippocampus, suggesting that tyrosine phosphorylation of tau precedes neuronal loss as well as motor/behavioral impairments, although it does not precede ser/thr phosphorylation. In contrast to JNPL3, the appearance of phospho-Tyr18 tau in the 3xTg mouse model was delayed relative to behavioral impairment and less well correlated with ser/thr phosphorylation. Our data indicates that tyrosine phosphorylation of tau has an integral role in the neurodegenerative process in JNPL3 and that activated Src family tyrosine kinases and cell cycle activation are involved as well.

Supplementary Material

Refer to Web version on PubMed Central for supplementary material.

Acknowledgments

We thank Drs. Frank M. LaFerla and Salvatore Oddo (University of California, Irvine, CA) for providing the triple transgenic mouse model for this study. We are also deeply indebted to Dr. Bruce Lamb for permitting a part of this study to be conducted at the Cleveland Clinic Foundation. We thank Dr. Peter Davies for antibodies (Alz50 and TG3) and Central Microscopy Research Facility (CMRF), University of Iowa, for their assistance in immunoelectron microscopy. This work was supported by National Institutes of Aging, AG17753 (to G.L.) and AG17216 (to S.H.Y.).

Funding

NIH AG17753 (to G.L.)

NIH AG117216 (to S.H.Y.)

References

1. Goedert M. Tau protein and the neurofibrillary pathology of Alzheimer's disease. Trends Neurosci. 1993; 16:460–5. [PubMed: 7507619]
2. Williamson R, Scales T, Clark BR, Gibb G, Reynolds CH, Kellie S, Bird IN, Varndell IM, Sheppard PW, Everall I, Anderton BH. Rapid tyrosine phosphorylation of neuronal proteins including tau and focal adhesion kinase in response to amyloid-beta peptide exposure: involvement of Src family protein kinases. J Neurosci. 2002; 22:10–20. [PubMed: 11756483]
3. Derkinderen P, Scales TM, Hanger DP, Leung KY, Byers HL, Ward MA, Lenz C, Price C, Bird IN, Perera T, Kellie S, Williamson R, Noble W, Van Etten RA, Leroy K, Brion JP, Reynolds CH, Anderton BH. Tyrosine 394 is phosphorylated in Alzheimer's paired helical filament tau and in fetal tau with c-Abl as the candidate tyrosine kinase. J Neurosci. 2005; 25:6584–93. [PubMed: 16014719]
4. Lee G, Thangavel R, Sharma VM, Litersky JM, Bhaskar K, Fang SM, Do LH, Andreadis A, Van Hoesen G, Ksiezak-Reding H. Phosphorylation of tau by fyn: implications for Alzheimer's disease. J Neurosci. 2004; 24:2304–12. [PubMed: 14999081]
5. Lebouvier T, Scales TM, Hanger DP, Geahlen RL, Lardeux B, Reynolds CH, Anderton BH, Derkinderen P. The microtubule-associated protein tau is phosphorylated by Syk. Biochim Biophys Acta. 2008; 1783:188–92. [PubMed: 18070606]
6. Shirazi SK, Wood JG. The protein tyrosine kinase, fyn, in Alzheimer's disease pathology. Neuroreport. 1993; 4:435–7. [PubMed: 8388744]
7. Ho GJ, Hashimoto M, Adame A, Izu M, Alford MF, Thal LJ, Hansen LA, Masliah E. Altered p59Fyn kinase expression accompanies disease progression in Alzheimer's disease: implications for its functional role. Neurobiol Aging. 2005; 26:625–35. [PubMed: 15708437]
8. Lambert MP, Barlow AK, Chromy BA, Edwards C, Freed R, Liosatos M, Morgan TE, Rozovsky I, Trommer B, Viola KL, Wals P, Zhang C, Finch CE, Krafft GA, Klein WL. Diffusible, nonfibrillar ligands derived from Abeta1-42 are potent central nervous system neurotoxins. Proc Natl Acad Sci U S A. 1998; 95:6448–53. [PubMed: 9600986]
9. Chin J, Palop JJ, Puolivali J, Massaro C, Bien-Ly N, Gerstein H, Scearce-Levie K, Masliah E, Mucke L. Fyn kinase induces synaptic and cognitive impairments in a transgenic mouse model of Alzheimer's disease. J Neurosci. 2005; 25:9694–703. [PubMed: 16237174]
10. Lee VM, Goedert M, Trojanowski JQ. Neurodegenerative tauopathies. Annu Rev Neurosci. 2001; 24:1121–59. [PubMed: 11520930]
11. Bhaskar K, Yen SH, Lee G. Disease-related modifications in tau affect the interaction between Fyn and Tau. J Biol Chem. 2005; 280:35119–25. [PubMed: 16115884]
12. Sahara N, Lewis J, DeTure M, McGowan E, Dickson DW, Hutton M, Yen SH. Assembly of tau in transgenic animals expressing P301L tau: alteration of phosphorylation and solubility. J Neurochem. 2002; 83:1498–508. [PubMed: 12472903]
13. Lewis J, McGowan E, Rockwood J, Melrose H, Nacharaju P, Van Slegtenhorst M, Gwinn-Hardy K, Paul Murphy M, Baker M, Yu X, Duff K, Hardy J, Corral A, Lin WL, Yen SH, Dickson DW,

Davies P, Hutton M. Neurofibrillary tangles, amyotrophy and progressive motor disturbance in mice expressing mutant (P301L) tau protein. Nat Genet. 2000; 25:402–5. [PubMed: 10932182]

14. Sharma VM, Litersky JM, Bhaskar K, Lee G. Tau impacts on growth-factor-stimulated actin remodeling. J Cell Sci. 2007; 120:748–57. [PubMed: 17284520]
15. Vincent I, Jicha G, Rosado M, Dickson DW. Aberrant expression of mitotic cdc2/cyclin B1 kinase in degenerating neurons of Alzheimer's disease brain. J Neurosci. 1997; 17:3588–98. [PubMed: 9133382]
16. Husseman JW, Nochlin D, Vincent I. Mitotic activation: a convergent mechanism for a cohort of neurodegenerative diseases. Neurobiol Aging. 2000; 21:815–28. [PubMed: 11124425]
17. Feddersen RM, Clark HB, Yunis WS, Orr HT. In vivo viability of postmitotic Purkinje neurons requires pRb family member function. Mol Cell Neurosci. 1995; 6:153–67. [PubMed: 7551567]
18. Park KH, Hallows JL, Chakrabarty P, Davies P, Vincent I. Conditional neuronal simian virus 40 T antigen expression induces Alzheimer-like tau and amyloid pathology in mice. J Neurosci. 2007; 27:2969–78. [PubMed: 17360920]
19. Andorfer C, Acker CM, Kress Y, Hof PR, Duff K, Davies P. Cell-cycle reentry and cell death in transgenic mice expressing nonmutant human tau isoforms. J Neurosci. 2005; 25:5446–54. [PubMed: 15930395]
20. Schindowski K, Belarbi K, Bretteville A, Ando K, Buee L. Neurogenesis and cell cycle-reactivated neuronal death during pathogenic tau aggregation. Genes Brain Behav. 2008; 7(Suppl 1):92–100. [PubMed: 18184373]
21. Khurana V, Lu Y, Steinhilb ML, Oldham S, Shulman JM, Feany MB. TOR-mediated cell-cycle activation causes neurodegeneration in a Drosophila tauopathy model. Curr Biol. 2006; 16:230–41. [PubMed: 16461276]
22. Gotz J, Chen F, van Dorpe J, Nitsch RM. Formation of neurofibrillary tangles in P301l tau transgenic mice induced by Abeta 42 fibrils. Science. 2001; 293:1491–5. [PubMed: 11520988]
23. Lewis J, Dickson DW, Lin WL, Chisholm L, Corral A, Jones G, Yen SH, Sahara N, Skipper L, Yager D, Eckman C, Hardy J, Hutton M, McGowan E. Enhanced neurofibrillary degeneration in transgenic mice expressing mutant tau and APP. Science. 2001; 293:1487–91. [PubMed: 11520987]
24. Oddo S, Caccamo A, Shepherd JD, Murphy MP, Golde TE, Kayed R, Metherate R, Mattson MP, Akbari Y, LaFerla FM. Triple-transgenic model of Alzheimer's disease with plaques and tangles: intracellular Abeta and synaptic dysfunction. Neuron. 2003; 39:409–21. [PubMed: 12895417]
25. Oddo S, Billings L, Kesslak JP, Cribbs DH, LaFerla FM. Abeta immunotherapy leads to clearance of early, but not late, hyperphosphorylated tau aggregates via the proteasome. Neuron. 2004; 43:321–32. [PubMed: 15294141]
26. Canlon B, Erichsen S, Nemlander E, Chen M, Hossain A, Celsi G, Ceccatelli S. Alterations in the intrauterine environment by glucocorticoids modifies the developmental programme of the auditory system. Eur J Neurosci. 2003; 17:2035–41. [PubMed: 12786969]
27. Xue M, Del Bigio MR. Comparison of brain cell death and inflammatory reaction in three models of intracerebral hemorrhage in adult rats. J Stroke Cerebrovasc Dis. 2003; 12:152–9. [PubMed: 17903920]
28. Vega IE, Cui L, Propst JA, Hutton ML, Lee G, Yen SH. Increase in tau tyrosine phosphorylation correlates with the formation of tau aggregates. Brain Res Mol Brain Res. 2005; 138:135–44. [PubMed: 15913839]
29. Braak E, Braak H, Mandelkow EM. A sequence of cytoskeleton changes related to the formation of neurofibrillary tangles and neuropil threads. Acta Neuropathol. 1994; 87:554–67. [PubMed: 7522386]
30. Gotz J, Chen F, Barmettler R, Nitsch RM. Tau filament formation in transgenic mice expressing P301L tau. J Biol Chem. 2001; 276:529–34. [PubMed: 11013246]
31. Ramsden M, Kotilinek L, Forster C, Paulson J, McGowan E, SantaCruz K, Guimaraes A, Yue M, Lewis J, Carlson G, Hutton M, Ashe KH. Age-dependent neurofibrillary tangle formation, neuron loss, and memory impairment in a mouse model of human tauopathy (P301L). J Neurosci. 2005; 25:10637–47. [PubMed: 16291936]

32. Lin WL, Lewis J, Yen SH, Hutton M, Dickson DW. Ultrastructural neuronal pathology in transgenic mice expressing mutant (P301L) human tau. J Neurocytol. 2003; 32:1091–105. [PubMed: 15044841]
33. Jicha GA, Bowser R, Kazam IG, Davies P. Alz-50 and MC-1, a new monoclonal antibody raised to paired helical filaments, recognize conformational epitopes on recombinant tau. J Neurosci Res. 1997; 48:128–32. [PubMed: 9130141]
34. Carmel G, Mager EM, Binder LI, Kuret J. The structural basis of monoclonal antibody Alz50's selectivity for Alzheimer's disease pathology. J Biol Chem. 1996; 271:32789–95. [PubMed: 8955115]
35. McKee AC, Carreras I, Hossain L, Ryu H, Klein WL, Oddo S, LaFerla FM, Jenkins BG, Kowall NW, Dedeoglu A. Ibuprofen reduces Abeta, hyperphosphorylated tau and memory deficits in Alzheimer mice. Brain Res. 2008; 1207:225–36. [PubMed: 18374906]
36. Oddo S, Caccamo A, Kitazawa M, Tseng BP, LaFerla FM. Amyloid deposition precedes tangle formation in a triple transgenic model of Alzheimer's disease. Neurobiol Aging. 2003; 24:1063–70. [PubMed: 14643377]
37. Zamora-Leon SP, Lee G, Davies P, Shafit-Zagardo B. Binding of Fyn to MAP-2c through an SH3 binding domain. Regulation of the interaction by ERK2. J Biol Chem. 2001; 276:39950–8. [PubMed: 11546790]
38. Mastrangelo MA, Bowers WJ. Detailed immunohistochemical characterization of temporal and spatial progression of Alzheimer's disease-related pathologies in male triple-transgenic mice. BMC Neurosci. 2008; 9:81. [PubMed: 18700006]
39. Hoerndli FJ, Pelech S, Papassotiropoulos A, Gotz J. Abeta treatment and P301L tau expression in an Alzheimer's disease tissue culture model act synergistically to promote aberrant cell cycle re-entry. Eur J Neurosci. 2007; 26:60–72. [PubMed: 17587323]
40. Billings LM, Oddo S, Green KN, McGaugh JL, LaFerla FM. Intraneuronal Abeta causes the onset of early Alzheimer's disease-related cognitive deficits in transgenic mice. Neuron. 2005; 45:675–88. [PubMed: 15748844]
41. Oddo S, Caccamo A, Cheng D, Jouleh B, Torp R, LaFerla FM. Genetically augmenting tau levels does not modulate the onset or progression of Abeta pathology in transgenic mice. J Neurochem. 2007; 102:1053–63. [PubMed: 17472708]

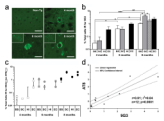

Fig. 1.

(a) Paraffin sections from 4, 6, and 8 month JNPL3 mouse brain (entorhinal cortex) were labeled with 9G3 and viewed by epifluorescence. Scale bar: 20μm. Insets at lower magnification show that 8 month old sample displayed increased number of phospho-Tyr18 tau positive cells relative to 6 month old. Phospho-Tyr18 tau immunoreactivity was lacking in 8-month-old non-transgenic mouse (upper left, scale bar: 30μm). **(b)** Phospho-Tyr18 tau appears at four months in three of the four brain regions and steadily increases with age in JNPL3 mice. Percentage of cells positive for 9G3 (number of positive cells divided by total number of cells examined in each brain region, as determined by Hoechst staining) was calculated from each animal (n=3). Values are expressed in mean percentage ±SEM. Comparisons were made between different brain regions within the same age group and for the same brain regions across different age groups. Differences that were statistically significant by unpaired t-test are indicated (*p<0.05; **p<0.01; ***p<0.005). BS-Brain Stem; SC-SubCortical structures; HI-Hippocampus; EC-Entorhinal Cortex **(c**) Correlation plot showing that the percentage of cells (mean+SEM) labeled for phospho-Tyr18 tau (squares) or AT8 (circles) increased with age in different brain regions of JNPL3 mice. AT8 or 9G3 positive cells were counted following single labeling. Individual markers (square or circle) within each age group represent the percentage of positive cells in brain stem (BS), subcortical structures (SC), hippocampus (HI) and entorhinal cortex (EC). Total number of cells examined per region (100%) was based on Hoechst staining. **(d)** Linear regression analysis between percentage of AT8 and 9G3 positive cells showed a significant correlation between 9G3 and AT8 immunoreactive cells in the different brain regions of each age group studied.

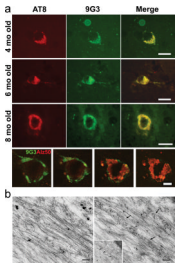

Fig. 2.

(a) Representative photomicrographs of the entorhinal cortices of 4-, 6- and 8-months-old JNPL3 mice brain showing cells double labeled with AT8 (red-left panel) and 9G3 (green-middle panel); merged images are shown in right panel. Scale bar: 20 μm. The bottom row shows four optical sections (9, 11, 14, 16) from a z-series stack of 22 optical sections (0.5μm thick) stained for 9G3 (green) and Alz50 (red) in the 8-month-old cortex. 9G3 positive tau was most abundant in sections 9-11 whereas Alz50 immunoreactive tau was most abundant in sections 14-16. Scale bar: 10 μm. **(b)** Post-embedding immunogold labeling with 9G3 showed 10nm gold particles decorating straight filaments (left) and filaments forming a herringbone pattern (right arrows) in ultrathin sections from JNPL3 spinal cord. Scale bar: 0.1μm.

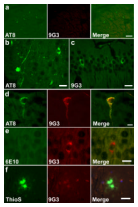

Fig. 3.

Appearance of phospho-Tyr18 tau in 3xTg mouse brain. **(a)** Each panel shows a confocal projection generated from z-series stack of 10 optical sections (0.5μm apart) AT8 immunoreactivity was observed in the fimbria region of 10 month old 3xTg brain. 9G3 labeling was absent. Scale bar: 30 μm. **(b)** AT8 immunoreactive dystrophic neurites were observed in the subiculum of 12 month old 3xTg brain. Scale bar: 20 μm. **(c)** 9G3 labeling was observed in the hippocampus. Scale bar: 20 μm. **(d)** Co-localization of AT8 and 9G3 was observed in 12 month old CA1 pyramidal neuron following double labeling with AT8 (green) and biotinylated-9G3 (red). Scale bar: 10 μm. **(e)** 9G3 positive CA1 hippocampal neurons lacked 6E10 intracellular Aβ staining. Scale bar: 15 μm. **(f)** Mature amyloid plaque, identified by Thio S, lacked 9G3 staining. Scale bar: 20 μm. (b-f) were viewed by epifluorescence microscopy.

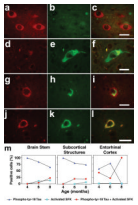

Fig. 4.

Representative photomicrographs from the brain stem of 8-month-old JNPL3 mouse showing cells immunoreactive for only activated SFK **(a-c)** or phospho-Tyr18 tau **(d-f)**. When activated SFK and phospho-Tyr18 appeared in the same cell in the entorhinal cortex, the subcellular distribution was either different **(g-i)** or overlapping **(jl)**. Scale bar: 20μm. **(m)** Percentage of positive cells immunoreactive for phospho-Tyr18 tau (9G3) alone (dark blue triangles), active-Src (pY416) alone (light blue squares) or for both (red circles) with increasing age in different brain regions of JNPL3 mice. The total number of positive cells per age group in respective brain regions was counted following double labeling with 9G3 and pY416 antibodies and assigned 100%. Hippocampus had no labeled cells at 4 and 6 months, then showed only double-labeled cells (both 9G3 and pY416 positive) at 8 months.

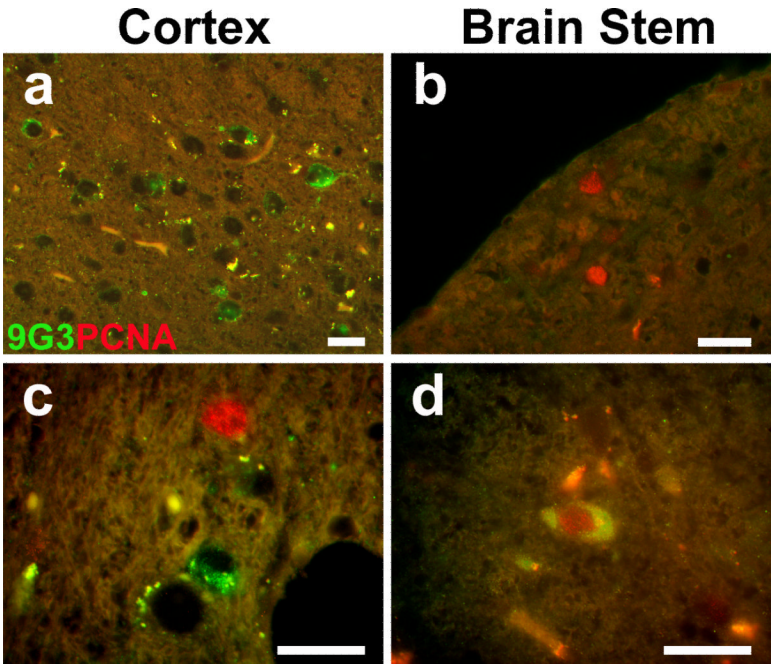

Fig. 5.

Partial overlap in the expression pattern of phospho-Tyr18 tau and PCNA in the JNPL3 mouse brain. Representative overlay images from 8-month-old JNPL3 double stained for phospho-tyr 18 (green) and PCNA (red) showed **(a)** cells immunoreactive for only phospho-Tyr18 tau in cortex, **(b)** cells immunoreactive for only PCNA in the brainstem, **(c)** both cell types in a single visual field in the cortex, and **(d)** cells immunoreactive for both phospho-Tyr18 and PCNA in the brainstem. Scale bar: 20μm.

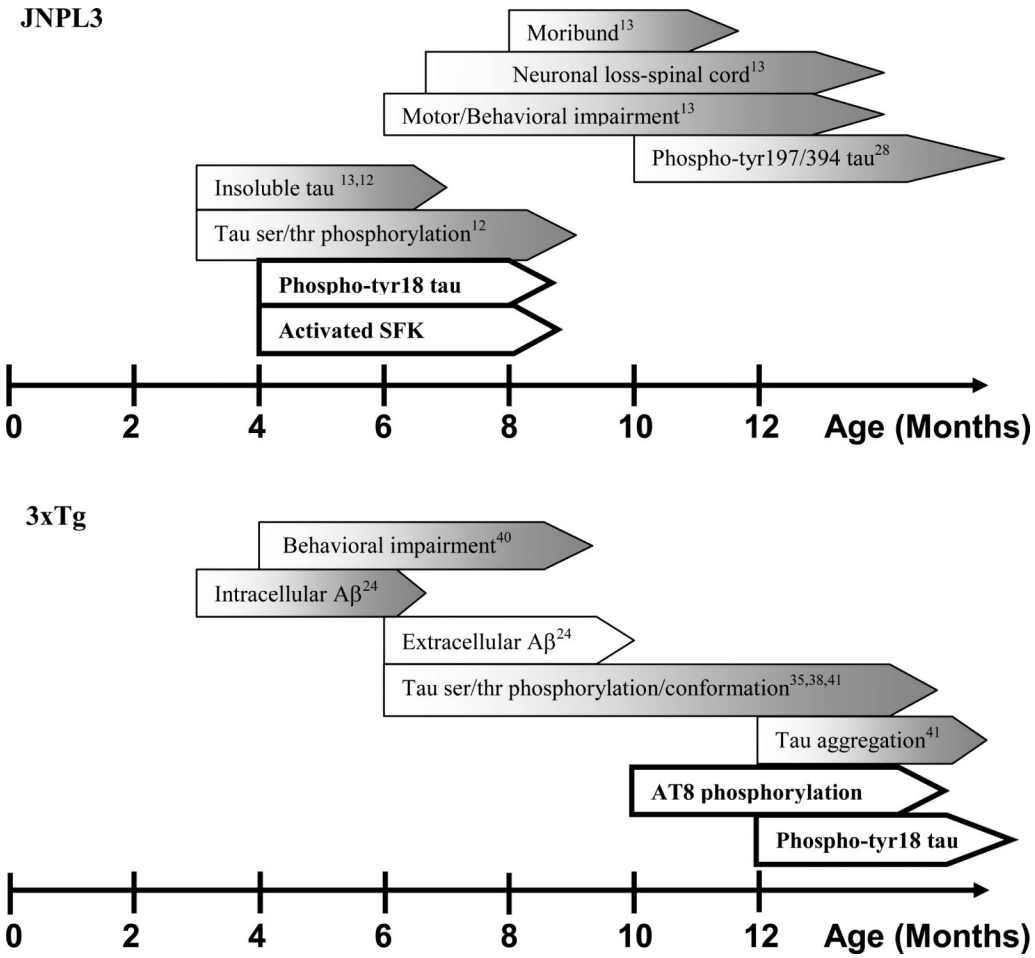

Fig. 6.

Summary of the relationship between phosphorylation of tau on Tyr18 and other attributes of JNPL3 (top) or 3xTg (bottom). Findings from this study are bolded.

Table 1

Quantification of cells positive for phospho-Tyr18 tau and/or PCNA

	Phospho-Tyr18 tau only (A)	PCNA only (B)	Phospho-Tyr18 tau + PCNA (C)	Fraction of Phospho-Tyr18 tau positive cells that are also positive for PCNA (D)
Brain stem	19.4 ± 2.8%	57.2 ± 20%	23.5 ± 8.77%	55%
Subcortical structures	53.9 ± 5.35%	35.8 ± 3.5%	10.2 ± 0.92%	16%
Hippocampus	53.5 ± 13.5%	30.7 ± 9.12%	15.8 ± 5.58%	23%
Entorhinal cortex	37.2 ± 3.49%	55.8 ± 6.2%	7.0 ± 0.69%	16%

For each brain region, the numbers of cells positive for only phospho-Tyr18 tau (9G3 positive), only Proliferating Cell Nuclear Antigen (PCNA), and for both were counted in 8-month-old JNPL3 mouse. The sum of the three types of labeled cells was assigned 100% and the contribution of each type of labeled cell to the sum is shown. That is, for each brain region, A + B + C = 100% where for example, A is the percentage of the total singly and doubly labeled cells that was positive only for 9G3. The column at the far right (D) shows the percent of 9G3 reactive cells that were positive for PCNA (C divided by [A + C]). The absolute number of immunoreactive cells in a given brain region was <4% of the total Hoechst positive cells per brain region examined. Numbers represent Mean±SEM (at least 5 sections per brain regions from n=3 animals).